Journal of Physical Science, Vol. 22(1), 25–37, 2011

Synthesis and Characterisation of Pure Nanoporous Hydroxyapatite

Rozita Ahmad Ramli[1], Rohana Adnan[1*], Mohamad Abu Bakar[1] and Sam'an Malik Masudi[2]

[1]School of Chemical Sciences, Universiti Sains Malaysia, 11800 USM Pulau Pinang, Malaysia
[2]School of Dental Sciences, Universiti Sains Malaysia, 16150 Kubang Kerian, Kelantan, Malaysia

*Corresponding author: r_adnan@usm.my

Abstract: *Hydroxyapatite (HA) is a desirable implant material due to its biocompatibility and osteoconductive properties. In this paper, we report a simple and economical approach to produce pure nanoporous HA using a hydroxyapatite-chitosan (HA-CS) template. The removal of chitosan through calcination leads to HA containing nanosize pores. Surface morphology analysis performed on both uncalcined and calcined HA-CS revealed disordered but interconnected pores. The removal of chitosan also resulted in a more even distribution of HA nanoparticles and a higher surface area. Both X-ray diffraction (XRD) and Fourier transform infrared (FTIR) analyses confirmed that the obtained material consisted of primarily highly crystalline noncarbonated hydroxyapatite.*

Keywords: hydroxyapatite, chitosan, blending, nanoporous, calcination, noncarbonated

Abstrak: *Hidroksiapatit (HA) adalah suatu bahan implan yang digemari kerana sifatnya yang bioserasi dan osteokonduktif. Artikel ini melaporkan pendekatan yang mudah dan ekonomikal untuk menghasilkan HA nanoporos tulen menggunakan templat hidroksiapatit-kitosan (HA-CS). Penyingkiran kitosan melalui pengkalsinan menghasilkan HA dengan liang bersaiz nano. Analisis morfologi permukaan yang dijalankan ke atas HA-CS yang tidak dikalsin dan dikalsinkan menunjukkan liang-liang yang tidak teratur tetapi saling berhubung. Penyingkiran kitosan juga menghasilkan nanozarah HA yang berserak rata dan berluas permukaan yang lebih tinggi. Kedua-dua analisis XRD dan FTIR menyokong bahawa bahan yang dihasilkan adalah terdiri daripada HA berhablur tinggi takberkarbonat.*

Kata kunci: hidroksiapatit, kitosan, pencampuran, nanoporos, pengkalsinan, takberkarbonat

1. INTRODUCTION

In this century, the production of materials with nanostructures has gained much attention for adsorption, catalytic, biomaterials and optical applications.[1–4] Hydroxyapatite (HA) is a material that has significant research

applications, especially in the biomedical field.[5] HA, with the chemical formula $Ca(PO_4)_6(OH)_2$, is the main component of bone and teeth.[6] Various methods have been employed for the preparation of HA either from natural sources (coral or bone)[7,8] or through chemical synthesis.[9–11] This bioceramic has been widely used in dental materials, constituent implants and bone substituent materials due to its excellent biocompatibility, bioactivity, osteoconductivity, non-toxicity and non-inflammatory nature.[12]

HA is manufactured in many forms and can be prepared as a dense ceramic,[13] powder,[14] ceramic coating[15] or porous ceramic[16] as required for the particular applications. However, in recent years, much research has been directed towards the development of porous HA for tissue engineering applications. Various techniques have been applied for the preparation of microporous HA structures, including hydrothermal conversion[17] and thermal spraying.[18] However, there are only a few reports concerning the preparation of nanoporous HA. HA with a nanoporous structure has been proven to enhance the cell adhesion, proliferation and differentiation required for tissue functions.[19] In fact, this nanoporous structure showed a much higher charging capacity, which is 16 times higher than that of commercially available and nonporous bioceramics.[20]

Generally, nanoporous HA can be prepared either with natural bone or a template. Murugan *et al*.[21] for example have reported the preparation of nanoporous HA from natural bovine bone. The bone was first chemically treated, followed by overnight calcination at 500°C. Although Murugan *et al*. prepared a bioceramic with an average pore size of 12 nm, the Fourier transform infrared (FTIR) results revealed the presence of carbonate ions in the calcined HA structure. Fan *et al*.[20] have synthesised nanoporous HA using mesoporous carbon as a template. The mesoporous carbon framework was then removed by combustion at 600°C for 5 hr. However, the X-ray diffraction (XRD) results clearly indicated that the obtained HA was mixed with β-tricalcium phosphate phases. Although these authors have successfully prepared nanoporous HA, the obtained HA was not pure. Impurities such as carbonate ions could affect the HA crystal structure, crystallinity and solubility,[21] thus limiting the application of HA, especially in biomedical applications.

It is therefore important to focus on the development of pure nanoporous HA. In this paper, we report a simple technique to produce pure nanoporous HA using HA-chitosan (CS) as a template. CS is the deacetylated product of chitin with a 2-amino-2-deoxy-D-glucose β-1,4 glycosidic linkage that is obtained primarily from seafood by-products.[22] Powder characterisation including phase composition, surface morphology and analysis of the pore size, is presented in this paper.

2. EXPERIMENTAL

2.1 Materials

The following chemicals were purchased and were used without further purification: calcium hydroxide ($Ca(OH)_2$, R&M Chemicals), orthophosphoric acid (H_3PO_4, 85% Ajax Chemicals), chitosan (80% deacetylation, Mw 1.50×10^5, Fluka) and aqueous ammonia solution (NH_3, 25% Merck).

2.2 Synthesis of Hydroxyapatite

HA crystals were synthesised by the co-precipitation method. A solution of 0.6 M H_3PO_4 was added dropwise to a 1 M $Ca(OH)_2$ aqueous solution under continuous stirring at room temperature. The final pH was adjusted to 11 by adding an ammonia solution. The resultant precipitate was aged for 24 hr under stirring. The white precipitate obtained was then collected by centrifugation and washed repeatedly with distilled water. The product was dried in an oven at 80ºC for 24 hr. The HA crystals obtained were ground with a mortar and pestle and then sieved at 45 µm. Finally, the HA crystals were calcined at 800ºC in a conventional furnace under an air atmosphere for 2 hr.

2.3 Synthesis of Nanoporous Hydroxyapatite

The HA-CS composite with a 20/80 (wt/wt) composition was prepared by the blending method. An aqueous CS solution was prepared by dissolving 0.4 g CS powder in 1 wt% acetic acid. Then, 0.1 g uncalcined HA obtained from the first reaction was dispersed completely in the CS solution under constant stirring for 1 hr at room temperature. The pH of the obtained HA-CS solution was adjusted to 11 by the addition of an ammonia solution. After stirring for 24 hr, the composite was centrifuged and washed repeatedly with distilled water, followed by freeze drying. Finally, the composite obtained was calcined under the same conditions as mentioned in the previous section.

2.4 Characterisation

HA and the HA-CS composite were analysed by powder XRD (Siemens D2000) with CuKα radiation over the 2θ range of 10–70° at intervals of 0.01° and with a count time of 0.5 s. Sample identification was made by comparing the diffraction patterns with PDF file no. 9–432. Infrared spectra in the range of 400–4000 cm^{-1} were recorded with a Perkin Elmer System 2000 using translucent pellets prepared by mixing powder samples with KBr. The particle morphology and pore size were evaluated by field emission scanning electron microscopy (FESEM, Leo Supra 50VP) and transmission electron microscopy (TEM, Philips

CM12). The specific surface area, pore size and pore volume were measured using a microporosimeter (Micromeritics ASAP 2010).

3. RESULTS AND DISCUSSION

Figure 1(a and b) show the SEM images of the HA-CS composite at low and high magnifications. From the figures, one can see that the interaction of HA and CS resulted in a scaffold structure with an average pore size of 26.7 ± 11.7 μm. The formation of a scaffolded HA-CS composite was expected due to the ability of CS to serve as a scaffolding matrix.

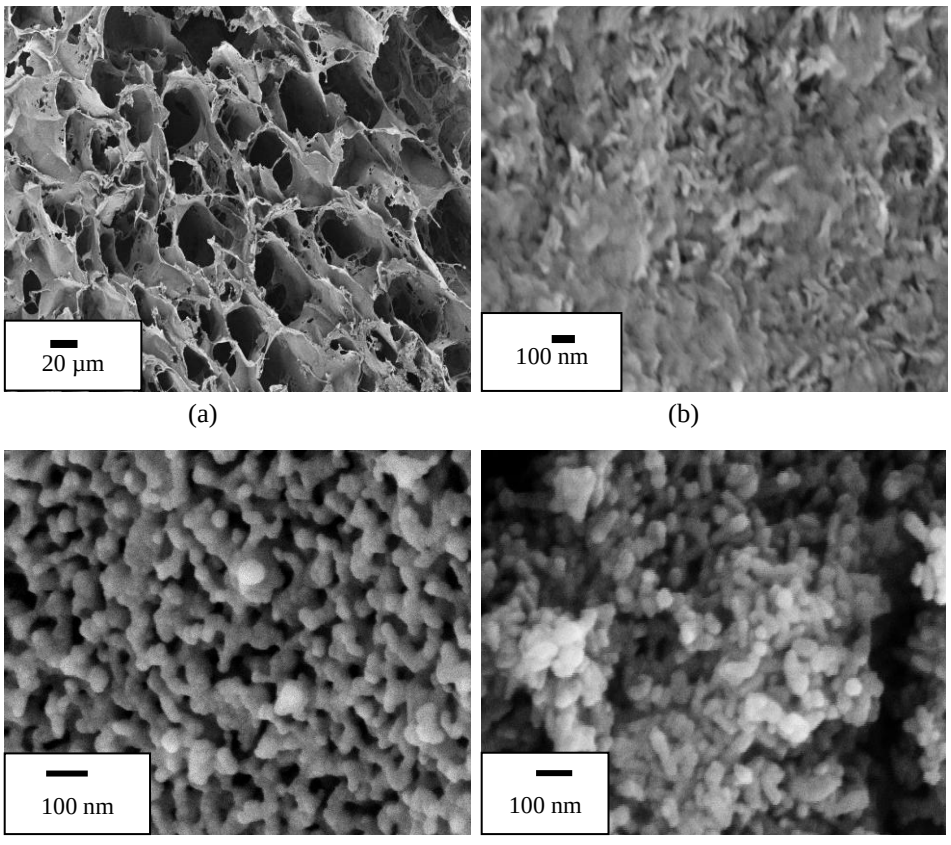

Figure 1: SEM micrographs of (a and b) the HA-CS composite, (c) the calcined composite and (d) calcined HA.

In this method, the composite was prepared in three steps. First, CS was dissolved in acetic acid to produce a CS solution. The dissolution process resulted in the protonation of the free amino group of CS (Equation 1) and in the transformation of the CS chain into a worm-like conformation. The reaction was then followed by blending HA crystals into the prepared CS solution. The HA particles easily penetrated and grew inside the CS matrix. The formation of the HA-CS crystals occurred as the pH of the solution varied. At this stage, the morphology of the composite obtained was significantly changed. This phenomenon was due to the modification of the CS conformation, which strongly depends on the pH of the environment. According to Rusu *et al*.,[24] the CS structure generally changes from worm-like to a more compact random coil conformation at higher pH values (3.5–5.6) and precipitates at a pH around 6.5–6.7 (Equation 2). This pH range leads to the formation of an interconnected three-dimension network between CS chains that can be approximated as a dendritic structure (Scheme 1a). The structure was greatly influenced by the CS content, with the use of more CS producing more dendritic structures. In this structure, HA crystallite seeds prefer to occupy and became stable when the pH of the environment was made alkaline (pH 10–11) (Equation 3, Scheme 1b).

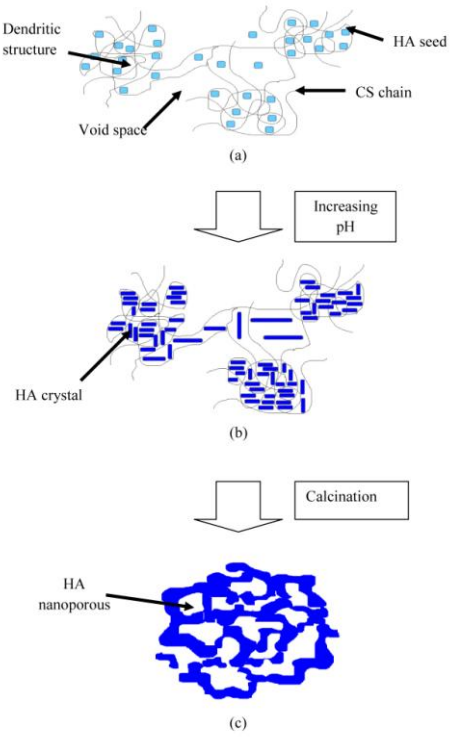

Scheme 1: Illustrating the synthesis of HA nanoporous by using HA-CS composite.

It has been reported that the formation of smaller HA crystals is favoured due to the limited spaces for the HA to grow. The crystals may have to rearrange accordingly, thus generating a cluster-like structure (Figure 1(b)). Excess water molecules were then removed during freeze drying, which leads to the formation of a scaffold and a porous structure (Figure 1(a)).

$$R\text{-}NH_2 + H^+ \rightarrow R\text{-}NH_3^+ \quad (1)$$

$$R\text{-}NH_3^+ + OH^- \rightarrow R\text{-}NH_2 (\downarrow) + H_2O \quad (2)$$

$$10Ca^{2+} + 6H_2PO_4^- + 14OH^- \rightarrow Ca_{10}(PO_4)_6(OH)_2 + 12H_2O \quad (3)$$

Figure 1(c) depicts the SEM images of the calcined HA-CS. As can be seen, the HA particles produced were evenly distributed with a porous structure. After the removal of CS through calcination, the retained HA crystals, which are thermally stable, contain disordered but interconnected nanosize pores.

The obtained morphology was also investigated by TEM images (Figure 2), which showed the presence of similar characteristics. The HA crystals produced by this method were observed to be smaller, shorter and more round in shape. According to Pang and Bao,[25] the calcination process affects not only the properties of the HA crystals but also the morphology of the particles. Generally, the formation of shorter and rounder HA crystals is favoured. To understand the role of CS as the template in the synthesis of nanoporous HA, neat sample of HA without CS was calcined under the same conditions. The results obtained clearly revealed that the calcined HA did not have a porous structure (Figure 1 (d)).

Figure 3 shows the nitrogen adsorption-desorption isotherms of the HA-CS composite, the calcined HA-CS composite and calcined HA, and Table 1 presents the summary of the isotherms results. The pore size and pore volume of the samples were obtained according to the Barrett-Joyner-Helenda (BJH) method, and the surface area was measured by the Brunauer-Emmett-Teller (BET) method.

Table 1: Summary of nitrogen adsorption/desorption results.

Sample	BET Surface area ($m^2\ g^{-1}$)	Pore size (nm)	Pore volume ($cc\ g^{-1}$)
HA-CS composite	16	12	0.0174
Calcined HA-CS composite	20	44	0.3450
Calcined HA	24	35	0.2264

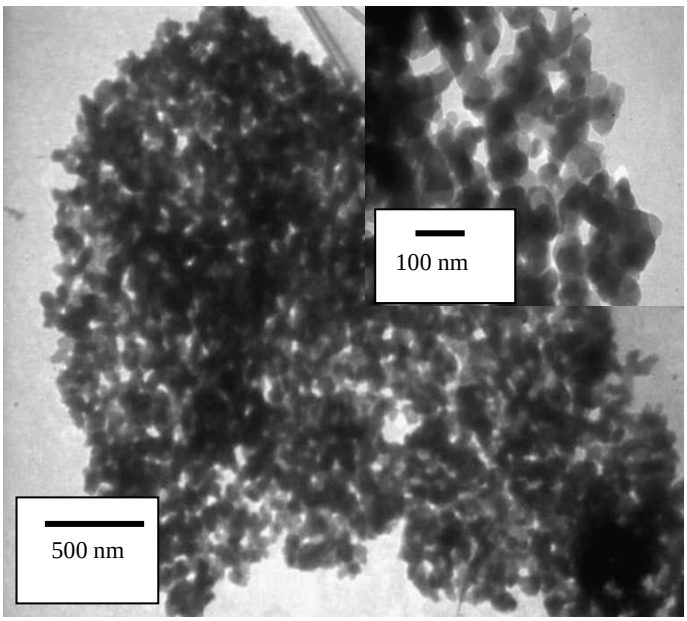

Figure 2: TEM image of the calcined HA-CS composite.

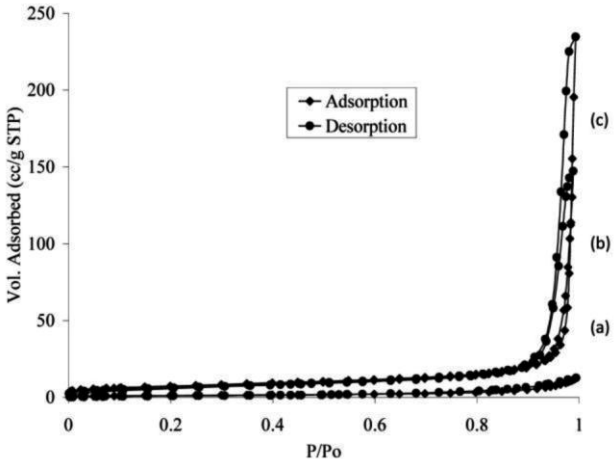

Figure 3: Nitrogen adsorption/desorption of (a) HA-CS composite, (b) calcined HA and (c) calcined HA-CS composite.

According to the results, all samples were predominantly mesoporous, as evidenced by the type IV isotherms.[26] However, both calcined HA and the calcined HA-CS composite exhibited higher hysteresis loops at $P/P_o > 0.8$ due to their higher surface areas. Interestingly, calcination of the composite increased the surface area by more than six times. Additionally, the calcined HA-CS

composite had a higher pore size and pore volume (44 nm and 0.3450 cc g^{-1}, respectively) than the nonporous calcined HA (35 nm and 0.2264 cc g^{-1}, respectively). However, there was no significant difference between the surface areas. We believe that the formation of the nanoporous structure contributed to this phenomenon, an idea that is supported by the SEM analysis.

The structural properties of all samples were further investigated by FTIR and XRD analysis. The FTIR spectra of the HA-CS composite, calcined HA-CS and calcined HA are given in Figure 4. The FTIR spectrum of the HA-CS composite (Figure 4(a)) showed all of the characteristic peaks of CS with additional peaks of apatite. Peaks corresponding to the chitosan aliphatic C-H stretching bands appeared in the 2877 cm^{-1} region. Meanwhile, the peaks at 1639 and 1258 cm^{-1} were assigned to the amino group (NH_2), which is one of the main functional groups of chitosan. The low-intensity peak identified at 1384 cm^{-1} was attributed to the C-O stretching mode of the primary alcohol group (CH_2-OH) of chitosan.[27] However, the presence of a high CS percentage in the composite complicates the characterisation of the apatite, as the broad bands from the two compounds overlap.

When the prepared HA-CS composite was calcined at 800°C, the CS components of the composite began to decompose at a temperature around 280–300°C.[28] The FTIR spectrum of the calcined HA-CS composite (Figure 4(b)) did not contain all of the peaks attributed to CS, while all of the characteristic peaks of pure HA were enhanced. The peaks at 569, 603, 963, 1045 and 1091 cm^{-1} were assigned to PO_4^{3-}, while the sharp peaks at 3570 and 633 cm^{-1} were due to the structural OH of the apatite.[25] For comparison, the FTIR spectrum of neat HA calcined at the same temperature and under the same conditions (Figure 4(c)) shows the typical characteristic peaks of B-type carbonated apatite[29] including the adsorption bands for CO_3^{2-} at 874, 1421 and 1466 cm^{-1}. It is known that the hydroxyl (OH^-) and the phosphate (PO_4^{3-}) sites in the HA lattice are hospitable towards carbonate ion (CO_3^{2-}) substitution, resulting in A-type or B-type apatites.[30,31] The incorporation of carbonate ions in the apatite structure is believed to have taken place during the preparation of HA, where the adventitious atmospheric CO_2 reacts with OH^- in the HA, forming carbonate ions[32] (Equation 4).

The FTIR analysis of the calcined HA-CS composite did not reveal any carbonate peaks. The lack of carbonate peaks is due to the acidic conditions employed during the preparation of the HA-CS composite.[33] Dissolution of the carbonate in the acidic medium takes place through protonation to form carbonic acid (H_2CO_3) (Equation 5),[34] and the subsequent calcination caused the decomposition of the carbonic acid into carbon dioxide gas and water Equation (6).

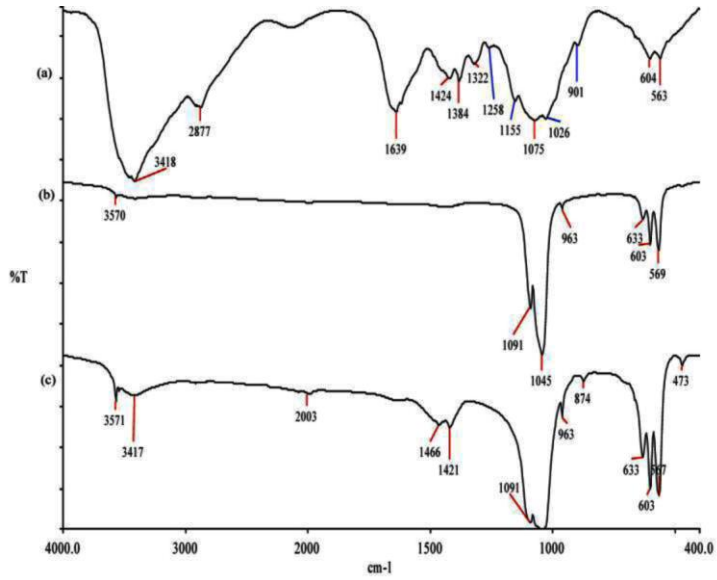

Figure 4: FTIR spectra of (a) HA-CS composite, (b) calcined HA-CS composite and (c) calcined HA.

Formation of carbonate ions:

$$CO_2 + 2OH^- \rightarrow CO_3^{2-} + H_2O \quad (4)$$

Removal of carbonate:

$$H^+ + HCO_3^- \rightarrow H_2CO_3 \quad (5)$$

$$H^+ + HCO_3^- \rightarrow H_2CO_3 \xrightarrow{\Delta} H_2O + CO_2 \quad (6)$$

Figure 5 shows the XRD diffractograms of the HA-CS composite, the calcined HA-CS composite and calcined HA. The XRD diffractograms of the HA-CS composite (Figure 5(a)) display broad peaks and poorly resolved superposed peaks. The CS peak was detected at approximately 20° (2θ), while HA peaks occurred in the 32–35° (2θ) region. Hence, the results of this investigation indicate that the formation of HA crystals in the CS matrix was greatly influenced by the high CS content used. This result was expected as a high CS composition was used for the preparation of the HA-CS composite. However, calcination treatment of the HA-CS composite resulted in prominently sharper diffraction peaks, which were attributed to a higher degree of crystallinity.[25] Consistent with the FTIR results, the XRD peaks of the calcined composite show that the CS peak was totally removed, leaving behind all of the characteristic peaks of HA (PDF file no. 9–432). The peaks of HA appearing at

26°, 30–34° and 40° (2θ) correspond to the (002), (102), (210), (211), (122), (300), (202) and (310) reflection planes. For comparison, calcined HA also showed the same XRD patterns as those of calcined HA-CS.

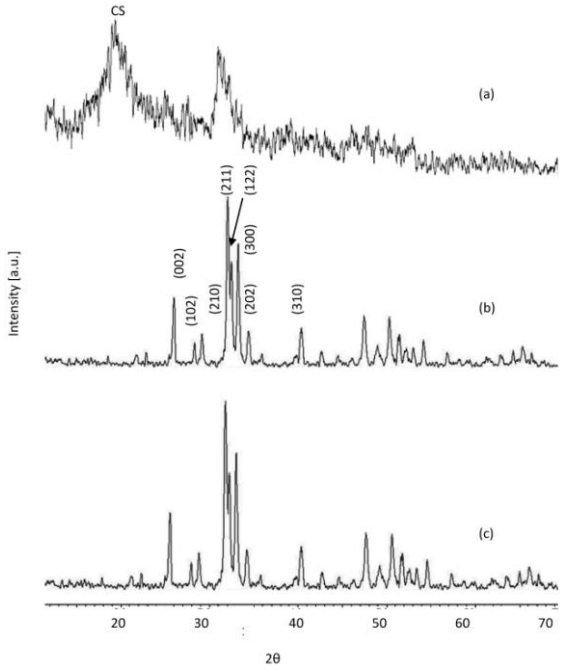

Figure 5: XRD diffractograms of (a) HA-CS composite, (b) calcined HA-CS composite and (c) calcined HA.

Both the FTIR and XRD analyses also revealed that the obtained nanoporous HA was pure and did not contain any carbonate ions. It has been reported that the solubility of carbonated HA is higher than that of pure HA, which leads to an increase in the rate of the demineralisation process.[36]

4. CONCLUSION

Hydroxyapatite (HA) containing nanosize pores was successfully synthesised through a simple and economical approach using a hydroxyapatite-chitosan template. The removal of chitosan by calcination resulted in a nanoporous material with a large surface area and a large pore size. The HA was also pure (i.e., noncarbonated), which was confirmed by Fourier transform infrared (FTIR) and x-ray diffraction (XRD) analysis.

5. ACKNOWLEDGEMENTS

The authors gratefully acknowledge the Universiti Sains Malaysia for a Graduate Assistanceship for R.A.R. and USM Short-Term Grant (304/PKIMIA/6310049).

6. REFERENCES

1. Zhang, H. Y., Shan, G., Liu, H. & Xing, J. (2007). Surface modification of γ-Al_2O_3 nano-particles with gum arabic and its applications in adsorption and biodesulfurization. *Surf. Coat. Technol.*, 201, 6917.
2. Dong, X., Wang, L., Deng, L., Li, J. & Huo, J. (2007). Preparation of nano-polyethylene fibres using Cp_2ZrCl_2/carbon nanotube catalytic system. *Mater. Lett.*, 61, 3111.
3. Kalita, S. M., Bhardwaj, A. & Bhatt, H. A. (2007). Nanocrystalline calcium phosphate ceramics in biomedical engineering. *Mater. Sci. Eng.*, C 27, 441.
4. Kim, J. & Song, K. (2007). Recent progress of nano-technology with NSOM. *Micron*, 38, 409.
5. Murugan, R. & Ramakrishna, S. (2005). Development of nanocomposites for bone grafting. *Comp. Sci. Technol.* 65, 2385.
6. LeGeros, R. Z. (1979). *Hydroxyapatite and related materials*, ed. Brown, P. W. & Constanz, B. Boca Raton: CRC Press.
7. Joschek, S., Nies, B., Krotz, R. & Gopfrerich, A. (2000). Chemical and physicochemical characterization of porous hydroxyapatite ceramics made of natural bone. *Biomaterials*, 21, 1645.
8. Jinawath, S., Polchai, D. & Yoshimura, M. (2002). Low-temperature, hydrothermal transformation of aragonite to hydroxyapatite. *Mater. Sci. Eng.*, C 22, 35.
9. Ito, A., Nakamura, S., Aoki, H., Akao, M., Teraoka, K., Tsutsumi, S., Onuma, K. & Tateishi, T. (1996). Hydrothermal growth of carbonate-containing hydroxyapatite single crystals. *J. Cryst. Growth*, 163, 311.
10. Saeri, M. R., Afshar, A., Ghorbani, M., Ehsani, N. & Sorrel, C. C. (2003). The wet precipitation process of hydroxyapatite. *Mater. Lett.* 57, 4064.
11. Kuriakose, T. A., Kalkura, S. N., Palanichamy, M., Arivuoli, D., Dierks, K., Bocelli, G. & Betzel, C. (2004). Synthesis of stoichiometric nano crystalline hydroxyapatite by ethanol-based sol-gel technique at low temperature. *J. Cryst. Growth*, 263, 517.

12. Rigo, E. C. S., Boschi, A. O., Yoshimoto, M., Allegrini Jr., S., Konig Jr., B. & Corbani, M. J. (2004). Evaluation in vitro and in vivo of biomimetic hydroxyapatite coated on titanium dental implants. *Mater. Sci. Eng.*, C 24, 647.
13. Kong, L. B., Ma, J. & Boey, F. (2002). Nanosized hydroxyapatite powders derived from coprecipitation process. *J. Mater. Sci.*, 37, 1131.
14. Kweh, S. W. K., Khor, K. A. & Cheang, P. (1999). The effect of processing parameters on the characteristics of plasma sprayed hydroxyapatite (HA) coatings. *J. Mater. Process. Technol.*, 89, 373.
15. Ben-Nissan, B., Milev, A. & Vago, R. (2004). Morphology of sol-gel derived nano-coated coralline hydroxyapatite. *Biomaterials*, 25, 4971.
16. Ozgur, N. E. & Cuneyt Tas, A. (1999). Manufacture of MacroPorous Calcium Hydroxyapatite and Tri-Calcium Phosphate Bioceramics. *J. Euro. Ceram. Soc.*, 19, 2569.
17. Xu, Y., Wang, D., Yang, L. & Tang, H. (2001). Hydrothermal conversion of coral into hydroxyapatite. *Mater. Charac.*, 47, 83.
18. Li, H., Khor, K. A. & Cheang, P. (2004). Thermal sprayed hydroxyapatite splats: nanostructures, pore formation mechanisms and TEM characterization. *Biomaterials*, 25, 3463.
19. Webster, T. J., Siegel, R. W. & Bizios, R. (2000). Enhanced functions of osteoblasts on nanophase ceramics. *Biomaterials*, 21, 1803.
20. Fan, J., Lei, J., Yu, C., Tu, B. & Zhao, D. (2007). Hard-templating synthesis of a novel rod-like nanoporous calcium phosphate bioceramics and their capacity as antibiotic carriers. *Mater. Chem. Phys*., 103, 489.
21. Murugan, R., Ramakrishna, S. & Rao, K. P. (2006). Nanoporous hydroxy-carbonate apatite scaffold made of natural bone. *Mater. Lett.*, 60, 2844.
22. Muzarelli, R. A. (1985). *The polysaccharides*, 417. New York: Academic Press.
23. Manjubala, I., Scheler, S., Bossert, J. J. & Jandt, K. D. (2006). Mineralisation of chitosan scaffolds with nano-apatite formation by double diffusion technique. *Acta Biomaterialia*, 2, 75.
24. Rusu, V. M., Ng, C., Wilke, M., Tiersch, B., Fratzi, P. & Peter, M. G. (2005). Size-controlled hydroxyapatite nanoparticles as self-organized organic-inorganic composite materials. *Biomaterials*, 26, 5414.
25. Pang, Y. X. & Bao, X. (2003). Influence of temperature, ripening time and calcination on the morphology and crystallinity of hydroxyapatite nanoparticles. *J. Euro. Ceram. Soc.* 23, 1697.
26. Lowell, S. (1979). *Introduction to Powder Surface Area*, 13. Toronto: John Wiley and Sons.
27. Murugan, R. & Ramakrishna, S. (2004). Bioresorbable composite bone paste using polysaccharide based nano hydroxyapatite. *Biomaterials*, 25, 3829.

28. Pang, X. & Zhitomirsky, I. (2005). Electrodeposition of composite hydroxyapatite-chitosan films. *Mater. Chem. Phys*. 94, 245.
29. Panda, R. N., Hsieh, M. F., Chung, R. J. & Chin, T. S. (2003). FTIR, XRD, SEM and solid state NMR investigations of carbonate-containing hydroxyapatite nano-particles synthesized by hydroxide-gel technique. *J. Phys. Chem. Solids,* 64, 193.
30. Fleet, M. E. & Liu, X. (2004). Location of type B carbonate ion in type A-B carbonate apatite synthesized at high pressure. *J. Solid State Chem.,* 177, 3175.
31. Moens, P., Callens, F., Matthys, P., Maes, F., Verbeeck, R. & Naessens, D. (1991). Adsorption of carbonate-derived molecules on the surface of carbonate-containing apatites. *J. Chem. Soc. Faraday Trans.*, 87, 3137.
32. Afshar, A., Ghorbani, M., Ehsani, N., Saeri, M. R. & Sorell, C. C. (2003). Some important factors in the wet precipitation process of hydroxyapatite. *Mater. Design,* 24, 197.
33. Madhavi, S., Ferraris, C. & White, T. J. (2005). Synthesis and crystallization of macroporous hydroxyapatite. *J. Solid State Chem.,* 178, 264.
34. Hankermeyer, R. C., Ohashi, K. L, Delancy, D. C., Ross, J. & Constantz, B. R. (2002). Dissolution rates of carbonated hydroxyapatite in hydrochloric acid. *Biomaterials,* 23, 743.
35. Baig, A. A., Fox, J. L., Hsu, J., Wang, Z., Otsuka, M., Higuchi, W. I. & LeGeros, R. Z. (1996). Effect of carbonate content and crystallinity on the metastable equilibrium solubility behavior of carbonated apatites. *J. Colloid Interface Sci.*, 179, 608.
36. Murugan, R. & Ramakrishna, S. (2006). Production of ultra-fine bioresorbable carbonated hydroxyapatite. *Acta Biomaterialia,* 2, 201.